2017-12-26

Tidal Conversion and Mixing Poleward of the Critical Latitude (an Arctic Case Study)

Rippeth, TP

10.1002/2017GL075310
Geophysical Research Letters
American Geophysical Union

AGU PUBLICATIONS

Geophysical Research Letters

RESEARCH LETTER
10.1002/2017GL075310

Key Points:
- The paper focuses on a region of significant tidal conversion and supercritical flow poleward of the critical latitude
- A modeling study predicts the generation of tidally generated high-frequency internal waves
- Observations show HF waves and associated dissipation indicating the waves as an energy pathway from tides to turbulence at high latitude

Correspondence to:
T. P. Rippeth,
t.p.rippeth@bangor.ac.uk

Citation:
Rippeth, T. P., Vlasenko, V., Stashchuk, N., Scannell, B. D., Green, J. A. M., Lincoln, B. J., & Bacon, S. (2017). Tidal conversion and mixing poleward of the critical latitude (an Arctic case study). *Geophysical Research Letters*, *44*. https://doi.org/10.1002/2017GL075310

Received 14 AUG 2017
Accepted 1 DEC 2017
Accepted article online 4 DEC 2017

Tidal Conversion and Mixing Poleward of the Critical Latitude (an Arctic Case Study)

Tom P. Rippeth[1], Vasiliy Vlasenko[2], Nataliya Stashchuk[2], Brian D. Scannell[1], J. A. Mattias Green[1], Ben J. Lincoln[1], and Sheldon Bacon[3]

[1]School of Ocean Sciences, Bangor University, Bangor, UK, [2]School of Biological and Marine Sciences, Plymouth University, Plymouth, UK, [3]National Oceanography Centre, Southampton, UK

Abstract The tides are a major source of the kinetic energy supporting turbulent mixing in the global oceans. The prime mechanism for the transfer of tidal energy to turbulent mixing results from the interaction between topography and stratified tidal flow, leading to the generation of freely propagating internal waves at the period of the forcing tide. However, poleward of the critical latitude (where the period of the principal tidal constituent exceeds the local inertial period), the action of the Coriolis force precludes the development of freely propagating linear internal tides. Here we focus on a region of sloping topography, poleward of the critical latitude, where there is significant conversion of tidal energy and the flow is supercritical (Froude number, $Fr > 1$). A high-resolution nonlinear modeling study demonstrates the key role of tidally generated lee waves and supercritical flow in the transfer of energy from the barotropic tide to internal waves in these high-latitude regions. Time series of flow and water column structure from the region of interest show internal waves with characteristics consistent with those predicted by the model, and concurrent microstructure dissipation measurements show significant levels of mixing associated with these internal waves. The results suggest that tidally generated lee waves are a key mechanism for the transfer of energy from the tide to turbulence poleward of the critical latitude.

Plain Language Summary The decline in aerial extent of sea ice covering the Arctic Ocean in the recent years is perhaps one of the leading indications of climate change. Warm water enters the Arctic Ocean at depths of 100–200 m; however, it is isolated from melting the ice by the lack of mixing in the Arctic Ocean. This lack of mixing has been attributed to the ocean being isolated from the wind by ice, and the fact that much of the Arctic Ocean is north of the critical latitude, beyond which the type of internal tide that is believed to drive mixing across other major oceans on the planet cannot occur. However, new evidence has been found that suggests that the tide might be important in driving mixing in certain areas of the Arctic Ocean. Here we combine state-of-the-art numerical modeling with new turbulence measurements to identify the mechanism by which the tide can drive mixing at these high latitudes.

1. Introduction

The tide plays a key role in global ocean circulation through the supply of mechanical energy to turbulence that stirs the ocean, promoting mixing (Munk & Wunsch, 1998). There has been much recent interest in the role of the tides in driving mixing in the climatically sensitive Arctic Ocean. Microstructure measurements of the rate of dissipation of turbulent kinetic energy (ε) have indicated significantly enhanced mixing over areas of sloping topography compared to the very quiescent conditions observed elsewhere in the Arctic Ocean (e.g., D'Asaro & Morison, 1992; Fer et al., 2010; Padman & Dillon, 1991; Rainville & Winsor, 2008). Rippeth et al. (2015) show that the enhanced levels of ε observed over the Arctic Ocean continental shelf break are correlated to the rate of conversion of barotropic tidal energy. This is an interesting result given that much of the Arctic Ocean lies poleward of the critical latitude, ϕ_c, at which the local inertial period matches the period of the principal semidiurnal tidal constituent (M2) (Figure 1). Stratified tidal flow over sloping topography can produce lee waves at any latitude. However, poleward of the critical latitude linear wave theory does not permit the generation of a freely propagating internal tide, the widely cited pathway for tidal energy conversion to turbulence in the ocean equatorward of the critical latitude (e.g., Green & Nycander, 2013).

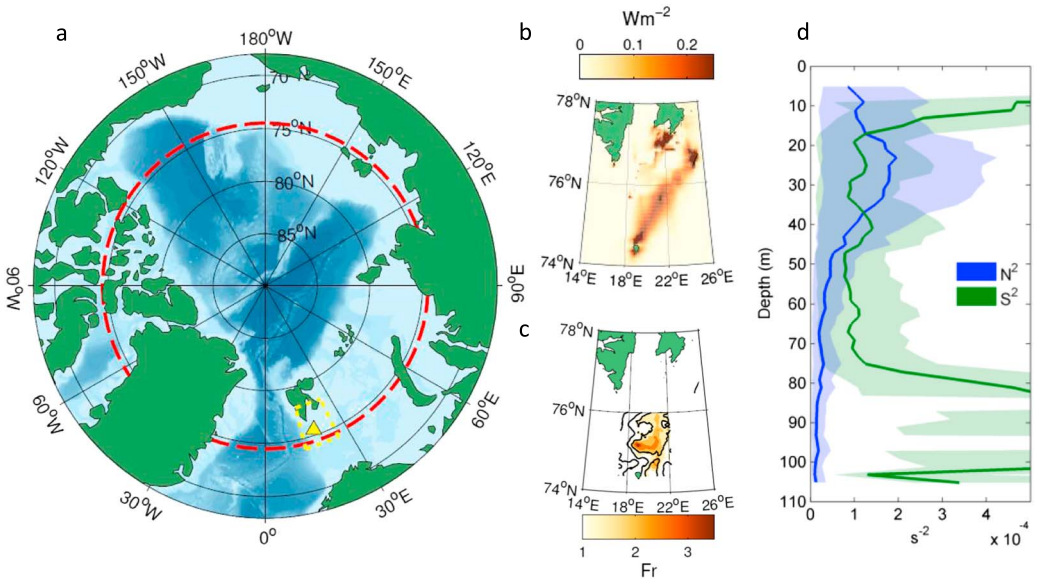

Figure 1. (a) A map of the Arctic Ocean showing the position of the observations (yellow triangle). The critical latitude at which the local inertial period matches the period of the principle semidiurnal tidal constituent (M2) is shown as a red dashed line. Lighter blue areas indicate shallower regions including continental shelf seas and ridges, while the darker blue areas indicate abyssal depths. (b) The area of interest (the box outlined by a yellow dotted line in Figure 1a) showing contours of the rate of conversion of tidal energy (W m^{-2}), in the M2 band, from the barotropic mode. (c) The Froude number distribution in the area of interest with bottom topography overlaid (black contours representing the 100, 200 and 300 m isobaths). (d) Mean profiles of buoyancy frequency (N^2) and vertical shear in the current speed (S^2) at the location of the observations. The mean is calculated for the 12 h period of the observations. The variability is shown by envelopes that represent the 95% confidence limits estimated by bootstrapping. These profiles indicate that the Gradient Richardson number over the thermocline region is close to one, and so the thermocline is of marginal stability.

Dynamically there are two principal mechanisms for tidal energy conversion from the barotropic to baroclinic modes over sloping topography. They are distinguished by the relative contribution of the two acceleration terms in the momentum balance equation:

$$\frac{d\mathbf{v}}{dt} = \frac{\partial \mathbf{v}}{\partial t} + (\mathbf{v} \cdot \nabla)\mathbf{v} \tag{1}$$

Here $\mathbf{v}$ is the velocity vector with components u, v, and w directed along the Ox, Oy, and Oz axes, respectively, in a Cartesian coordinate system with the (xy) plane placed on the undisturbed free surface and the z axis directed vertically upward.

In a linear approximation with an assumption of weak tidal activity when only small-amplitude waves are generated (see, e.g., Falahat & Nycander, 2015; Nycander, 2005), the second term in the right-hand side of equation (1) is neglected and the governing system for plane waves in an inviscid fluid is reduced to a single wave equation (Vlasenko et al., 2005):

$$w_{xx} - \frac{\sigma^2 - f^2}{N^2(z) - \sigma^2} w_{zz} = 0 \tag{2}$$

Here $f = 2\Omega \sin(\phi)$ is the Coriolis parameter, Ω is the angular frequency of the Earth's rotation, ϕ is latitude, $N(z)$ is the buoyancy frequency such that $N^2(z) = -(g/\rho)(\partial\rho/\partial z)$, where g is the acceleration due to gravity, ρ the water density, and σ is the tidal frequency.

In systems with weak rotation ($f < \sigma < N$), equation (2) is hyperbolic, with solutions that represent progressive internal waves of tidal frequency radiated from the source as freely propagated waves. However, in systems with strong rotation ($f > \sigma$), including latitudes poleward of ϕ_c—which is 74.5° for the semidiurnal M2 tidal constituent—the equation becomes elliptic, and solutions represent evanescent waves decaying exponentially away from the source. Excluding the nonlinear terms in equation (1) therefore results in a prediction

that rotation will significantly reduce the conversion of energy from the barotropic tide to the baroclinic internal tide poleward of ϕ_c. However, the nonlinear terms may actually contribute to tidal energy conversion through the tide-topography interaction (Bell, 1975; Nakamura & Awaji, 2000; Nakamura et al., 2000). Vlasenko et al. (2005) show that the advective term in equation (1) can lead to the generation of unsteady lee waves. The properties of these waves are very different to those of long baroclinic tidal waves, as they occur as packets of high-frequency internal waves with a spatial scale of the same order as the bottom topographic features. They are generated by tidal currents on the lee side of the sloping bottom topography. As the down slope current accelerates, the waves are trapped, forming a type of hydraulic jump. Vlasenko et al. (2003) suggest that this "lee jump" formation as a potential mechanism for conversion of tidal energy poleward of the critical latitude. Here we use "lee wave" to mean the structure described above, rather than propagating internal waves generated by a general (nontidal) flow.

The aim of this paper is to demonstrate that lee wave generation coupled with supercritical barotropic tidal flow over sloping topography is a key mechanism for the transfer of energy from the tide to turbulent mixing poleward of the critical latitude. To achieve this, we will combine evidence from a proof of concept high-resolution numerical modeling study with new in situ observations of profiles of the rate of dissipation of turbulent kinetic energy (ε) from a region of significant tidal conversion and supercritical tidal flow poleward of the critical latitude.

2. Region of Interest

The focus of the present study is the Spitsbergen Bank, a shallow bank to the east of the Fram Strait and south of Svalbard that is poleward of the critical latitude ϕ_c (Figure 1). A 12 h time series of measurements were made here on the 8 August 2013, a couple of days ahead of a spring tide. These measurements included profiles of water column structure, velocity, and ε made at a location on the edge of the bank (75° 30′; Figure 1a).

The rate of conversion of barotropic tidal energy over the region is expressed as a local balance between the rate of work done by the tide generating force and the divergence in the tidal energy flux (Egbert & Ray, 2001). The rate of tidal conversion is the sum of the rates of energy transfer to baroclinic modes and to dissipation in the bottom boundary layer. Here it is computed using tidal amplitudes and currents from the TPX08 database (available from volkov.oce.orst.edu/tides/tpx08_atlas.html). Figure 1b shows that the region of interest is an area of significant conversion of barotropic tidal energy. The water column was stratified with warmer (6.8°C), fresher (34.53) water overlying cooler (3.5°C), saltier (34.93) water at the time of the measurements with maximum stratification between approximately 20 m and 40 m (Figure 1d).

A necessary condition for unsteady lee wave generation is that the Froude number, $Fr = U/c$, where U is the tidal velocity and c is the phase speed of internal waves, should exceed the critical threshold value of 1. The phase speed c of the internal waves is found by solving the eigenvalue problem:

$$\begin{aligned} \Phi_{zz} + \frac{N^2(z)}{c_j^2}\Phi_j &= 0 \\ \Phi(-H) = \Phi(0) &= 0 \end{aligned} \tag{3}$$

where $\Phi_j(z)$ is the eigenfunction that defines the vertical structure of jth internal mode, c_j is the phase speed of the internal mode, and $j = 1, 2, 3, \ldots$ is the mode number.

A Froude number analysis was carried out for the region, using the background stratification measured during August 2013 (Figure 1d) and the maximum velocity of the semidiurnal M2 tide from the TPX08. The phase speed of the first internal mode for different depths was then calculated using (3). The distribution of the Froude number is shown in Figure 1c and reveals that most of the study area, including all areas where the depth is less than 100 m, is supercritical for tidal flow and so potentially susceptible to unsteady lee wave formation through tide-topography interaction.

3. Numerical Modeling Study

The aim of the modeling study is to show that the barotropic tidal currents are able to generate internal waves in the region of interest (i.e., poleward of the critical latitude) and to characterize the internal wavefield. To achieve this we use the fully nonlinear nonhydrostatic Massachusetts Institute of Technology

general circulation model (MITgcm, Marshall et al., 1997) to simulate the tidally generated internal waves in the region.

A two-dimensional version of the model was configured with fine resolution: 1 m in the vertical and 9 m in the horizontal direction. The horizontal grid step was exponentially increased near lateral boundaries to provide nonreflectance of radiated waves from the boundaries for at least five tidal periods. Tidal forcing was applied in the model by a tidal potential added to the right-hand side of the momentum balance equations. The amplitudes of the zonal and meridional velocities in tidal ellipses were set to 0.3 m s^{-1} at 100 m depth. The N^2 profile was calculated from mean profiles of temperature and salinity (Figure 1d). A bank topography profile with slopes typical of those found along the transect was used. The horizontal viscosity and diffusivity were set to be constant at 0.01 m^2 s^{-1}, which, in conjunction with the small horizontal grid step, provided reasonable conditions for the reproduction of the details of the generation processes. A Richardson number dependent parametrization for vertical viscosity ν and diffusivity κ (Pacanowski & Philander, 1981) was used:

$$\nu = \frac{\nu_0}{(1+\alpha Ri)^n} + \nu_b$$
$$\kappa = \frac{\nu}{(1+\alpha Ri)} + \kappa_b \quad (4)$$

Here Ri is the gradient Richardson number, $Ri = N^2(z)/S^2(z)$; $\nu_b = 10^{-5}$ m^2 s^{-1} and $\kappa_b = 10^{-5}$ m^2 s^{-1} are the background parameters; $\nu_0 = 1.5 \times 10^{-2}$ m^2 s^{-1}, α=5, and n=1 are the adjustable parameters. This parameterization increases the coefficients ν and κ in the areas where the Richardson number is small, to account for mixing processes induced by shear instability and breaking internal waves.

4. Generation Mechanism

The model results show the generation of packets of high-frequency waves over the topography that are initially trapped but propagate away as the tide slackens. The generation and the evolution of the high-frequency internal wave packets over several tidal cycles is shown in Figure 2. At the beginning of the cycle (Figure 2a), the tidal flow moves across the topography and elevates the isotherms on the upstream side of the topography (identified as zone A) and depresses them on the downstream side (i.e., on the lee side, identified as zone B). The resulting elevated and depressed features (identified as a1 and b1) are trapped while the flow is supercritical. As the tide weakens and the flow becomes subcritical the features, a1 and b1, are able to propagate away from the topography. The reversing tidal flow then accelerates, becoming supercritical, resulting in the generation of a second set of features (a2 and b2) that develop and are trapped as illustrated in the Hovmöller diagram (Figure 2b).

The generation process is repeated on every tidal cycle. As the features propagate they evolve into packets of high-frequency internal waves radiating away from the topography as shown in Figure 2c. The Hovmöller diagram (Figure 2d) shows the evolution and propagation of the internal wave packets over two further tidal cycles. The leading edge of the internal wave packets propagating to the left is linked by red dotted lines, with the corresponding trailing edge indicated by a black dashed line illustrating a spatial scale for the wave packet of about 5 km. The leading edge of the waves propagating to the right is linked by a dotted green line with the corresponding trailing edge again indicated by the black dotted line. The model therefore predicts that the supercritical tidal flow over the topography generates two packets of high-frequency internal waves per tidal cycle, which then radiate away. However, the wave packets propagating against the tide are held by the flow.

To illustrate the characteristics of the waves from the perspective of single point measurements, we show the predicted evolution of the temperature structure at two fixed points, V1 and V2, away from the topography in Figure 3. From this perspective there is evidence of two types of waves at both locations. The first is a long-period, semidiurnal wave that is present at both locations but smaller in amplitude at the location farthest from the topography (V2). This is consistent with linear theory that predicts the existence of only evanescent modes poleward the critical latitude.

The second type of waves evident is packets of high-frequency internal waves that occur at the same point of every tidal cycle. The high-frequency internal waves are present at a particular location for 3–5 h during each semidiurnal tidal cycle. These waves are characterized by a larger-amplitude (approximately 10 m) wave followed by a series of smaller-amplitude waves with a period of 20–30 min.

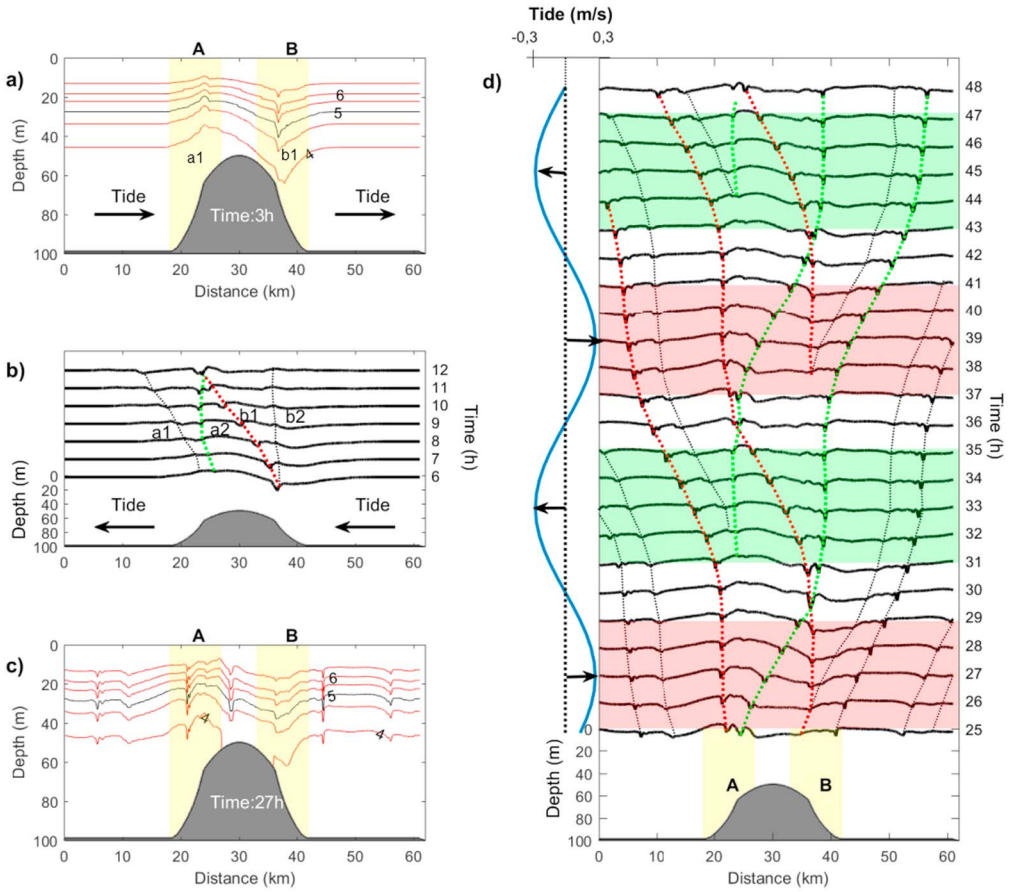

Figure 2. Simulated temperature fields (4–6.5°C isotherms at 0.5°C intervals) after (a) 3 and (c) 27 h of model time. The Hovmöller diagrams showing evolution of the 5° isotherm during the simulation time periods of (b) $t = 6–12$ h and (d) t=25–48 h. The contour interval represents 1 h. Green and red dotted lines identify the features radiating away from the topography. The direction and strength of the tidal flow is shown by a blue solid line. The red and green shaded areas show time intervals with supercritical ($Fr > 1$) conditions for radiated internal waves. Generation zones A and B are shaded yellow in Figures 2a, 2c, and 2d.

In order to determine the partitioning of tidal energy conversion between the evanescent linear tidal wave and the unsteady lee wave the model was also run for identical conditions but with the nonlinear terms turned off. A comparison between the linear and nonlinear cases shows that the energy transfer to nonlinear internal waves accounts for 71% of the total tidal conversion. It should be noted that while a sensitivity analyses of the partitioning of the energy transfer between the linear and nonlinear waves is beyond the scope of this paper, the ratio is likely to be very sensitive to the Froude number of the flow.

5. Observations

A 12 h time series of velocity and turbulence profile data were collected on the edge of the bank along a short transect that approximately followed the 100 m contour. The north-south transect was repeated over two successive 6 h periods (approximately 3 km in length). As the ship moved slowly forward, a set of microstructure observations was made using a loosely tethered Rockland VMP500 microstructure profiler (VMP) that profiled from approximately 10 m below the sea surface to the sea bed. Simultaneous current profiles were taken using an RDI 300 kHz acoustic Doppler current profiler attached to the stern of the ship, which collected data with a 2 m bin size and single ping observations every 2 s. The barotropic tide over this area was found to be elliptical with the major axis oriented approximately east-west with maximum $U \sim 0.4\ \mathrm{m\ s^{-1}}$, and the minor axis oriented approximately north-south with maximum $V \sim 0.3\ \mathrm{m\ s^{-1}}$.

The first transect took place between 07.00 and 13.00 GMT with 41 VMP profiles collected. At this time the direction of the barotropic tide was predominantly westward, oriented approximately off-bank. The second

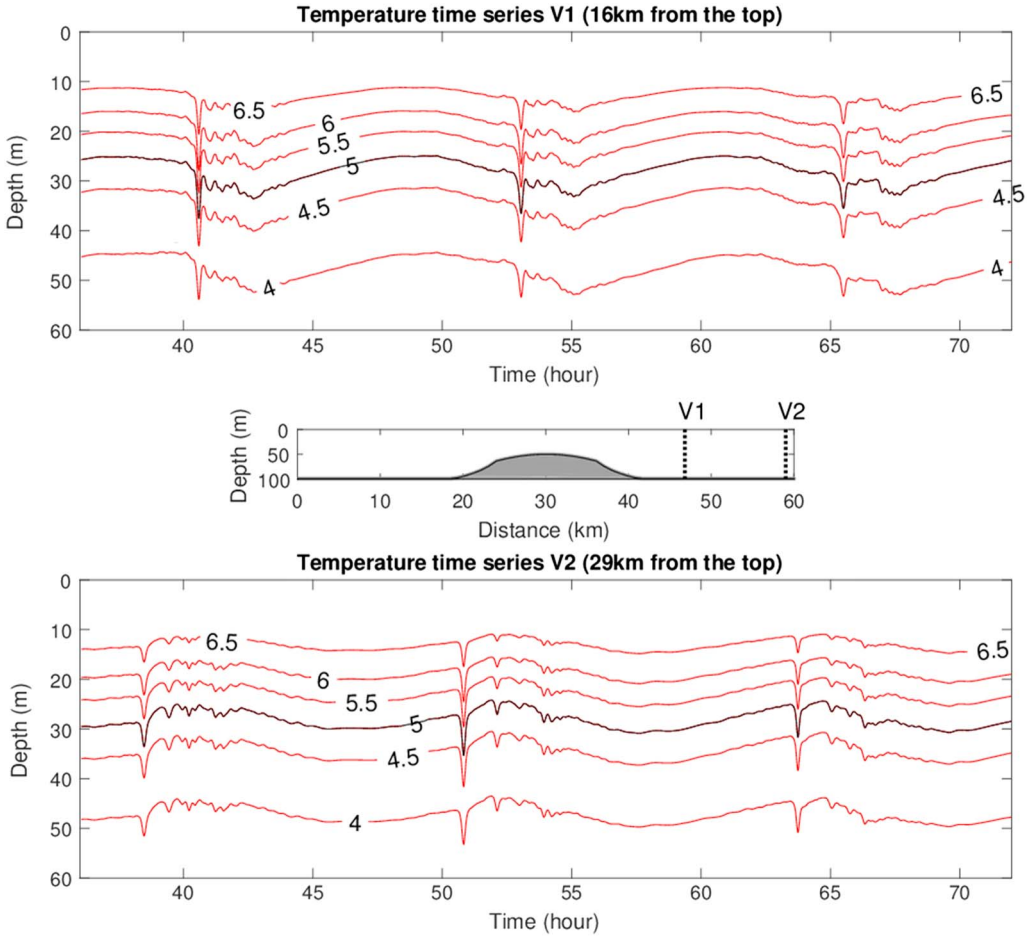

Figure 3. Temperature time series predicted by the model at two fixed points, V1 (16 km from the top of the topography) and V2 (29 km from the top of the topography). The positions relative to the topography are shown in the middle panel. The 4–6.5°C isotherms are shown at 0.5°C intervals.

transect took place when the flow was oriented predominantly on-bank, between 14.00 and 19.00 GMT, during which time 47 VMP profiles were collected. During both transects VMP profiles were taken approximately every 6 min providing profiles of temperature, salinity (and hence density), and ε (e.g., Rippeth et al., 2015), with gaps during the first transect and between the first and second transects while the ship repositioned.

Mean profiles show that the gradient Richardson number is approximately 1, indicating the water column is susceptible to shear instability (Figure 1d). The time series of temperature, ε, and the observed midwater currents are presented together with the shear in the horizontal velocities across the thermocline, in Figure 4. During the first transect the thermocline is relatively thin, widening from 10 to 20 m when defined by the 4.5 and 6°C isotherms. There are intermittent displacements in the isotherms of up to 15 m with periods of 20–30 min. These features are particularly apparent from about 09:00 to the gap in the data after 10:00, and again around 12:00.

During the second transect the thermocline again thickens, with the separation of the 4.5 and 6°C isotherms increasing from 15 to 30 m over the duration of the transect. From about 15.00 h to the end of the time series there are seven internal waves evident, with the amplitude of the leading wave about 15 m and the following waves about 5–10 m. The period of the waves is approximately 30 min. Estimates of shear in the horizontal velocities, across the thermocline (Figure 4b), indicate variability of up to an order of magnitude, with the peaks in shear occurring approximately every 30 min, and so correlated with the vertical movement of the isotherms associated with the presence of internal waves.

A time series of the vertical distribution of ε is shown in Figure 4c. High values of ε are evident close to the boundaries, and in particular in the bottom boundary layer. Within the thermocline there is high temporal

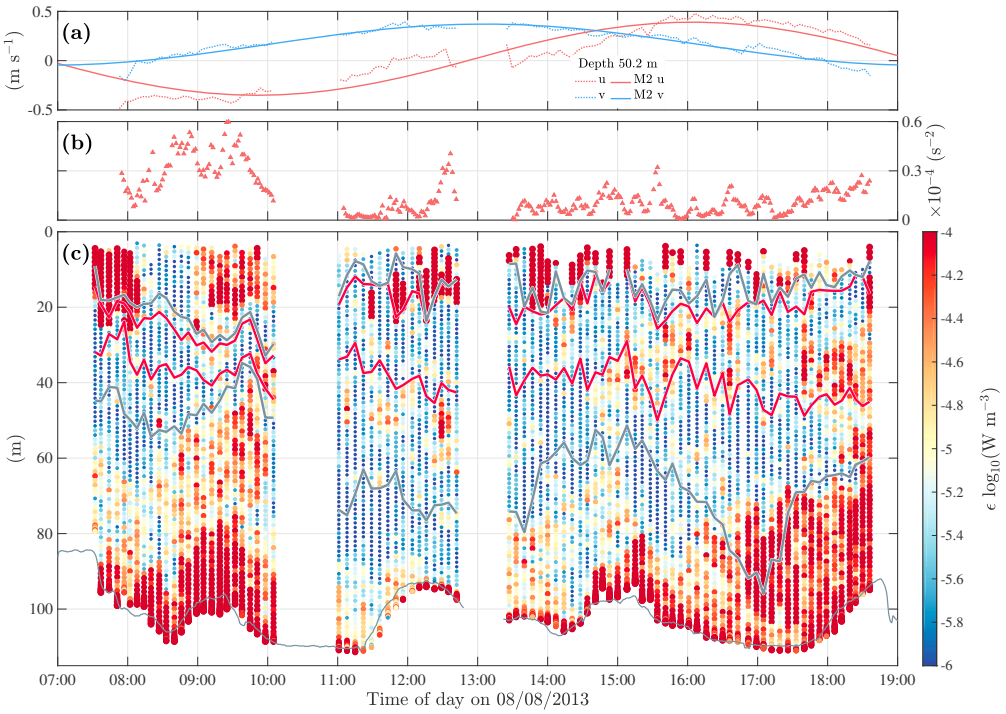

Figure 4. (a) Observed velocity (dotted line) together with the tidal current velocity predicted through tidal analysis (solid line) in the eastward (red, approximately on-bank) and northerly (blue) directions at a middepth location (50 m). (b) Vertical shear in the horizontal velocity across the thermocline evaluated between 10 m depth-averages centered around 8.15 m and 68.15 m with 240 s running average at 100 s intervals based on raw observations at 2 s intervals and 2 m depth bins. (c) The colored dots represent measurements of ε from VMP profiles taken approximately every 6 min; the red lines are the 4.5 and 6°C isotherms; and the grey lines indicate the surface mixed layer and bottom boundary layer based on a maximum temperature difference of 0.4°C from the boundary value, with ε values between the grey lines indicating dissipation within the thermocline.

variability in ε with isolated patches of enhanced dissipation, which coincide with the periods of significant internal wave activity. The mean thermocline ε over the period of the second transect is 4.5×10^{-5} W m^{-3} with several periods of significant enhancement evident (e.g., around 15:00 and 16:00 coincident with isotherm displacements of up to 15 m and spikes in the shear) and toward the end of the transect. Water column-integrated estimates of dissipation imply that the total dissipation is dominated by bottom boundary layer dissipation, although the total observed dissipation in the thermocline (i.e., between the bottom boundary layer and the surface mixed layer) accounted for 37% (bootstrap 95% confidence limits of 28 to 49%) of the dissipation observed below the surface mixed layer.

6. Discussion

Recent observations have shown continental shelf break regions of the Arctic Ocean host significant barotropic tidal energy conversion (Rippeth et al., 2015), with evidence of greatly enhanced ε, and by implication mixing, over sloping topography in the presence of significant tides (e.g., D'Asaro & Morison, 1992; Fer et al., 2010; Padman & Dillon, 1991; Rainville & Winsor, 2008; Rippeth et al., 2015). This is in sharp contrast to much of the central Arctic Ocean that is found to be remarkably quiescent (e.g., Lincoln et al., 2016; Shibley et al., 2017). However, much of the Arctic Ocean lies poleward of the critical latitude and so the conversion of barotropic tidal energy to a freely propagating linear internal tide, over sloping topography, is suppressed by rotation.

In this paper we present a mechanism for tidal energy conversion poleward of the critical latitude, in which supercritical tidal flows result in the transfer of energy to short length-scale internal lee waves that are generated over steep topography as a result of strong nonlinear advection. The mechanism is demonstrated through a high-resolution nonlinear numerical modeling study focused on a region of sloping topography in the vicinity of the Spitsbergen Bank, an area identified as hosting significant barotropic tidal conversion, and

where the tidal flow is supercritical ($Fr > 1$). The modeling study predicts that for the conditions found in this area at this time approximately 71% of the barotropic tidal energy converted to baroclinic modes is associated with the nonlinear internal waves while the remainder is associated with an evanescent semidiurnal internal tide. It is worth noting that the nonlinear wave component is not currently included in the tidal mixing parameterization (Falahat & Nycander, 2015) available for application in locations poleward of the critical latitude.

A 12 h time series of temperature and velocity profiles collected on the edge of the Spitsbergen Bank reveal the presence of high-frequency internal waves with coincident enhancement of shear and characteristics similar to those predicted by the model. Coincident ε profiles reveal that water column integrated dissipation is dominated by dissipation close to the boundaries, with the tidally generated bottom boundary layer accounting over half of the observed ε. This would suggest that a significant proportion of the converted tidal energy is dissipated within the well-mixed bottom boundary layer and so not available to support mixing. Approximately a third of the observed ε occurs within the stratified midwater column and so will potentially contribute to mixing.

The observed thermocline mean ε is comparable to those previously reported over the continental shelf break to the north of Svalbard (e.g., Rippeth et al., 2015) and is similar to those reported over sloping topography for regions of similar water depths and tidal currents, equatorward of the critical latitude (e.g., Rippeth, 2005). While the high spatial and temporal variability of dissipation, and therefore mixing, associated with the lee wave energy transfer mechanism evident from the modeling study, imply that the resolution of the observations reported here fails to fully resolve the associated mixing, they do indicate the potential of this mechanism to contribute to mixing. Evidence of the spatial extent of this energy conversion mechanism comes from recent studies based on Envisat synthetic aperture radar images that show the existence of high-frequency internal waves across large areas of the eastern Arctic (Kozlov et al., 2014, 2015).

The analysis presented highlights that the barotropic tidal conversion alone is not a good estimator of mixing for a number of reasons. The partitioning of converted energy between the evanescent internal tide and the nonlinear internal waves will vary considerably according to local flow conditions. Furthermore, the proportion of the converted energy dissipated in the bottom boundary layer (and so not available to mix the water column) is also likely to vary greatly. However, the Froude number may be a useful diagnostic in the prediction of the location and evolution of mixing hot spots poleward of the critical latitude. Accordingly changes in both stratification and flow over topography could result in the development of supercritical flow, and consequently mixing, as reported for lower latitudes (Stephenson et al., 2015). There are large seasonal changes in the stratification in the Arctic. Furthermore, there is evidence of increased currents associated with sea ice loss (Giles et al., 2012). These changes will impact both the tidal conversion rate and the partitioning of energy between the linear and nonlinear modes and so lead to variations in both the magnitude of, and spatial and temporal patterns in, tidally driven midwater column mixing.

Acknowledgments

T. P. R., V. V., and N. S. contributed equally to the writing of this paper. Data collection and analysis by B. J. L. and T. P. R. was funded through the UK NERC TEA-COSI Consortium (PI: SB, NE/I028947/1). B. D. S. is supported by NERC award 1500369 through the Envision DTP. J. A. M. G. acknowledges NERC funding from FASTNEt (NE/I030224/1) and RidgeMix (NE/L004216/1). We thank the officers, crew, and principal scientist of the *RRS James Clark Ross* cruise 288, supported by the NERC ACCACIA consortium. T. P. R. and B. J. L. planned the field work while B. J. L. lead the data collection. J. A. M. G., B. J. L., and B. D. S. all contributed to data analysis. V. V. and N. S. carried out the numerical modeling. The observations reported in this paper are available on request from British Oceanographic Data Centre, National Oceanography Centre, Liverpool (http://www.bodc.ac.uk).

References

Bell, T. H. (1975). Lee waves in stratified flows with simple harmonic time dependence. *Journal of Fluid*, *67*(4), 705–722.

D'Asaro, E. A., & Morison, J. H. (1992). Internal waves and mixing in the Arctic Ocean. *Deep Sea Research Part II*, *39*, 459–484.

Egbert, G. D., & Ray, R. D. (2001). Estimates of M2 tidal energy dissipation from TOPEX/Poseidon altimeter data. *Journal of Geophysical Research*, *106*(10), 22,475–22,502.

Falahat, S., & Nycander, J. (2015). On the generation of bottom-trapped internal tides. *Journal of Physical Oceanography*, *45*, 526–545.

Fer, I., Skogseth, R., & Geyer, F. (2010). Internal waves and mixing in the Marginal Ice Zone near Yermak Plateau. *Journal of Physical Oceanography*, *40*(7), 1613–1630.

Giles, K. A., Laxon, S. W., Ridout, A. L., Wingham, D. J., & Bacon, S. (2012). Western Arctic Ocean freshwater storage increased by wind-driven spin-up of the Beauford Gyre. *Nature Geoscience*, *5*, 194–197. https://doi.org/10.1038/ngeo1379

Green, J. A. M., & Nycander, J. (2013). A comparison of tidal conversion parameterization for tidal models. *Journal of Physical Oceanography*, *43*, 104–119.

Kozlov, I., Kudryavtsev, V., Zubkova, E., Atadzhanova, O., Zimin, A., Romanenkov, D., … Chapron, B. (2015). SAR observations of internal waves in the Russian Arctic Seas. In *Proc. IGAARS Symposium* (pp. 947–949). IEEE.

Kozlov, I., Romanenkov, D., Zimin, A., & Chapron, B. (2014). SAR observing large-scale non-linear internal waves in the White Sea. *Remote Sensing of Environment*, *147*, 99–107.

Lincoln, B. J., Rippeth, T. P., Lenn, Y.-D., Timmermans, M. L., Williams, W. J., & Bacon, S. (2016). Wind-driven mixing at intermediate depths in an ice free Arctic Ocean. *Geophysical Research Letters*, *43*, 9749–9756. https://doi.org/10.1002/2016GL070454

Marshall, J., Adcroft, A., Hill, C., Perelman, L., & Heisey, C. (1997). A finite-volume, incompressible Navier-Stokes model for studies of the ocean on the parallel computers. *Journal of Geophysical Research*, *102*, 5733–5752.

Munk, W. H., & Wunsch, C. (1998). Abyssal recipe II: Energetics of tidal and wind mixing. *Deep Sea Research Part I*, *45*, 1977–2010.

Nakamura, T., & Awaji, T. (2000). The growth mechanism for topographic internal waves generated by an oscillatory flow. *Journal of Physical Oceanography*, *31*, 2511–2524.

Nakamura, T., Awaji, T., Hatayame, T., Akimoto, K., Takizawa, T., Kono, T., … Fukasawa, M. (2000). The generation of large-amplitude unsteady lee waves by subinertial K1 tidal flow: A possible vertical mixing mechanism in the Kuril Straits. *Journal of Physical Oceanography*, *30*, 1601–1621.

Nycander, J. (2005). Generation of internal waves in the deep ocean by tides. *Journal of Geophysical Research*, *110*, C10028. https://doi.org/10.1029/2004JC002487

Pacanowski, R. C., & Philander, S. G. H. (1981). Parameterisation of vertical mixing in numerical models of tropical oceans. *Journal of Physical Oceanography*, *11*, 1443–1451.

Padman, L., & Dillon, T. M. (1991). Turbulent mixing near Yermak Plateau during the coordinated eastern Arctic experiment. *Journal of Geophysical Research*, *96*, 4769–4782.

Rainville, L., & Winsor, P. (2008). Mixing across the Arctic Ocean: Microstructure observations during the Beringia 2005 expedition. *Geophysical Research Letters*, *35*, L08606. https://doi.org/10.1029/2008GL033532

Rippeth, T. P. (2005). Mixing in seasonally stratified shelf seas: A shifting paradigm. *Philosophical Transactions of the Royal Society A*, *363*, 2837–2854. https://doi.org/10.1098/rsta.2005.1662

Rippeth, T. P., Lincoln, B. J., Lenn, Y.-D., Green, J. A. M., Sundfjord, A., & Bacon, S. (2015). Tide-mediated warming of Arctic halocline by Atlantic heat fluxes over rough topography. *Nature Geoscience*, *8*, 191–194.

Shibley, N. C., Timmermans, M. L., Carpenter, J. R., & Toole, J. M. (2017). Spatial variability of the Arctic Ocean's double-diffusive staircase. *Journal of Geophysical Research*, *122*, 980–994. https://doi.org/10.1002/2016JC012419

Stephenson, G. R., Hopkins, J. E., Green, J. A. M., Inall, M. E., & Palmer, M. R. (2015). Wind-mixing by storms modifies baroclinic energy flux on the Celtic Sea shelf. *Geophysical Research Letters*, *42*, 1826–1833. https://doi.org/10.1002/2014GL062627

Vlasenko, V., Stashchuk, N., & Hutter, K. (2005). *Baroclinic tides: Theoretical modeling and observational evidence* (365 pp.). Cambridge, UK: Cambridge University Press.

Vlasenko, V., Stashchuk, N., Hutter, K., & Sabinin, K. D. (2003). Nonlinear internal waves forced by tides near the critical latitude. *Deep Sea Research Part I*, *50*, 317–338.